

**SCHOOL OF MATERIALS AND MINERAL RESOURCES ENGINEERING  
UNIVERSITI SAINS MALAYSIA**

**FORMATION OF HIERARCHICAL POROUS IRON OXIDE AND THEIR  
APPLICATION IN REDUCING Cr(VI)**

By

**ONG YEE CHIN**

**Supervisor: Associate Professor Dr. Zainovia Lockman**

Dissertation submitted in partial fulfillment  
of the requirements for the degree of Bachelor of Engineering with Honours  
(Materials Engineering)

Universiti Sains Malaysia

**JUNE 2017**

## DECLARATION

I hereby declare that I have conducted, completed the research work and written the dissertation entitled “**Formation of Hierarchical Porous Iron and Their Application in Reducing Cr(VI)**”. I also declare that it has not been previously submitted for the award for any degree or diploma or other similar title of this for any other examining body or University.

Name of Student : ONG YEE CHIN

Signature:

Date : 3<sup>rd</sup> July 2017

Witnessed by

Supervisor : Assoc. Prof.Dr. Zainovia Lockman

Signature:

Date : 3<sup>rd</sup> July 2017

## **ACKNOWLEDGEMENTS**

Here I would like to express my most sincere appreciation to those people who had helped me along this project. Without them this project would not be completed. Firstly, I would like to sincerely thank my supervisor, Associate Professor Dr. Zainovia Lockman for her guidance, advice and support to bring this research project to fruition. She is a good teacher to me and always provide me useful advice on my experimental and thesis work.

I gratefully appreciate School of Materials and Mineral Resources Engineering, Universiti Sains Malaysia (USM) for providing required environment and equipment to perform my research. Without School of Materials and Mineral Resources Engineering, this research title will not be able to complete. Also, completing this work would have been all more difficult were it not for the support provided by the technical staffs of the School of Materials and Mineral Resources Engineering. I am indebted to them for their help.

Besides, I would like to convey my appreciation to Dr. Zainovia's research team for providing the necessary help as well as the valuable advice on the experimental work, whenever I needed.

I also would like to thank all my friends, my beloved parents and also my sisters for their kindness and mental support during my study especially. Thanks for their endless love, support and encouragement.

## TABLE OF CONTENTS

<b>Contents</b>	<b>Page</b>
DECLARATION	ii
ACKNOWLEDGEMENTS	iii
TABLE OF CONTENTS	iv
LIST OF TABLES	vii
LIST OF FIGURES	viii
LIST OF ABBREVIATIONS	ix
LIST OF SYMBOLS	xiii
ABSTRAK	xiv
ABSTRACT	xvi
<b>CHAPTER 1 INTRODUCTION</b>	<b>1</b>
1.1 Background	1
1.2 Removal of Cr(VI) from Water Bodies	2
1.3 Nanomaterials	6
1.4 Iron Oxide as Photocatalysts	7
1.5 Problem Statement	9
1.6 Objectives	11
1.7 Scopes of Work	11
1.8 Outline of Chapters	11
<b>CHAPTER 2 LITERATURE REVIEW</b>	<b>13</b>
2.1 Introduction	13
2.2 Basics of Chromium	13
2.3 Chromium in Nutrition and Its Effect to Human	15
2.4 Remediation of Cr(VI)	15
2.3.1 Ion Exchange	16

2.3.2	Chemical Precipitation	17
2.3.3	Electrochemical Treatment	17
2.3.4	Membrane Filtration	18
2.3.6	Photocatalytic Technology	19
2.3.7	Cr(VI) Removal by Iron Oxide	22
2.4	Nanostructure Oxide Material	23
2.5	Hierarchical Structure	25
2.6	Nanomaterials Synthesis Process	28
2.7.1	Hematite	30
2.7.2	Magnetite	31
2.7.3	Maghemite	31
2.8	Formation of Iron Oxide Nanostructures	31
2.8.1	Thermal Oxidation of Iron	32
2.8.2	Mechanism of Growth of Iron Oxide Nanostructure	38
2.8.3	Presence of Water Vapour in Oxidation of Iron	42
<b>CHAPTER 3      METHODOLOGY</b>		44
3.1	Introduction	44
3.2	Methodology	45
3.2.1	Effect of Oxidation Temperature	47
3.2.2	Effect of Presence of Water Vapour	47
3.2.3	Effect of Oxidation Time	49
3.3	Characterization Techniques	49
3.3.1	Field Emission Scanning Electron Microscopy (FESEM)	50
3.3.2	Transmission Electron Microscopy (TEM)	50
3.3.3	X-Ray Diffraction (XRD)	51
3.3.4	Raman Spectroscopy	51
3.3.5	UV-Visible Spectrophotometer (UV-VIS)	52

3.4	Photocatalysis Experiment	52
3.4.1	Preparation of Chromium Stock Solution	52
3.4.2	Photocatalysis Experiment	52
3.4.3	Photocatalysis Analysis	53
<b>CHAPTER 4</b>	<b>RESULTS AND DISCUSSION</b>	<b>55</b>
4.1	Introduction	55
4.2	Hierarchical Porous Iron Oxide Formation by Thermal Oxidation	55
4.2.1	Effect of Oxidation Temperature and Water Vapour	56
4.2.2	Effect of Oxidation Time	63
4.2.3	Thermal Oxidation of Iron Foil	67
4.3	Growth Mechanism of Nanostructure Iron Oxide	71
4.3.1	Initial Oxidation	71
4.3.2	Oxidation Scale Formation	73
4.3.3	Self-assembly of Nanostructure	77
4.4	Photocatalysis of Cr(VI) on Iron Oxide Nanostructures	80
<b>CHAPTER 5</b>	<b>CONCLUSION AND RECOMMENDATION</b>	<b>97</b>
5.1	Conclusion	97
5.2	Recommendations	98
<b>REFERENCES</b>		<b>99</b>

## LIST OF TABLES

		<b>Page</b>
Table 2.1	General properties of chromium (Lepora, 2005).	13
Table 2.2	Comparison of Cr(VI) remediating techniques (Madhavi et al., 2013, Barrera-Díaz et al., 2012).	21
Table 2.3	Comparison of photocatalytic reduction performance of different photocatalyst on Cr(VI)	23
Table 2.4	Comparison of synthesis approaches for nanomaterials.	28
Table 2.5	Properties of iron oxides (Cornell and Schwertmann, 2006).	29
Table 2.6	Summary of works on thermal oxidation of iron.	37
Table 2.7	Summary of oxidation of iron in presence of water vapour.	43
Table 3.1	List of materials used for this project.	45
Table 3.2	Summary of parameters used in studying the effect of oxidation temperature.	47
Table 3.3	Summary of the parameters used in studying effect of presence of water vapour.	48
Table 3.4	Summary of parameters used for effect of oxidation time.	49
Table 4.1	Raman band positions of $\alpha$ -Fe <sub>2</sub> O <sub>3</sub> , $\gamma$ -Fe <sub>2</sub> O <sub>3</sub> and Fe <sub>3</sub> O <sub>4</sub>	62
Table 4.2	Pilling-Bedworth Ratio of iron oxide (Yuan et al., 2012)	77
Table 4.3	Reduction percentage of Cr(VI) with different samples	91
Table 4.4	Comparison of several works with present study on Cr(VI) reduction	92
Table 4.5	Comparison of microstructure of iron wire oxidised at 500 °C for (a) 15, (b) 30 and (c) 60 minutes	96

## LIST OF FIGURES

		<b>Page</b>
Figure 1.1	Photocatalysis on a semiconductor (Philippopoulos and Nikolaki, 2010).	4
Figure 1.2	Iron oxides in the global system (Cornell and Schwertmann, 2006).	5
Figure 1.3	Types of iron oxides.	6
Figure 1.4	Classification of nanomaterials.	7
Figure 2.1	Pourbaix diagram for chromium species (Kotaś and Stasicka, 2000).	14
Figure 2.2	Schematic illustration of ion exchange process.	16
Figure 2.3	Schematic illustration of chemical precipitation method.	17
Figure 2.4	Schematic illustration of electrochemical treatment process.	18
Figure 2.5	Schematic diagram of membrane filtration technique.	18
Figure 2.6	Photocatalysis under sunlight irradiation.	20
Figure 2.7	FESEM images of flower-like structure developed in Fe-glycolate (Lim et al., 2016).	26
Figure 2.8	Shape evolution of the structures of iron oxide at different temperatures (Zhao et al., 2017)	26
Figure 2.9	SEM images of morphologies of iron oxides (Zhang et al., 2005).	27
Figure 2.10	SEM images of the wafers with (a) low, (b) medium and (c) high magnifications (Basu et al., 2009).	27
Figure 2.11	Crystal structure and crystallographic data of the hematite, magnetite and maghemite (the black ball is Fe <sup>2+</sup> , the green ball is Fe <sup>3+</sup> and the red ball is O <sup>2-</sup> ) (Wu et al., 2015).	30
Figure 2.12	Cross section FESEM images of iron oxidised at (a) below 570 °C and (b) above 570 °C (Budiman et al., 2016).	32
Figure 2.13	SEM nanowires images: a) curl-shaped morphology b) aligned nanowire arrays (Fu et al., 2001).	33
Figure 2.14	(a) SEM image of hematite nanowires and (b) TEM image shows the bicrystalline nature and amorphous edges. (c) Raman spectrum and (d) XRD of the same sample (Hiralal et al., 2008).	34
Figure 2.15	Oxide layers of iron (a) optical microscope image with circles denote approximate areas of Raman measurements); (b) SEM image of	

	different iron oxide layers. Raman spectra of iron oxide layers from the indicated measurement points: (c) $\alpha$ -Fe <sub>2</sub> O <sub>3</sub> , (d) Fe <sub>3</sub> O <sub>4</sub> and (f) FeO (Nasibulin et al., 2009).	35
Figure 2.16	FESEM images of iron oxidised at (a) 500 °C and (b) 800 °C (Budiman et al., 2016).	35
Figure 2.17	XRD patterns of film grown in (a) water and (b) ethanol (Zhang et al., 2005).	36
Figure 2.18	XRD patterns of (a) $\alpha$ -Fe <sub>2</sub> O <sub>3</sub> , (b) Fe <sub>3</sub> O <sub>4</sub> and (c) $\gamma$ -Fe <sub>2</sub> O <sub>3</sub> (Zhong et al., 2006).	37
Figure 2.19	Schematic illustration of the growth of nanowires and the inset shows the stacking fault defects in [110] direction (Nasibulin et al., 2009).	40
Figure 2.20	Schematic diagram of diffusion of iron for growth of nanowires: outward diffusion of iron ions to stress free surface through grain boundary diffusion then surface diffusion of iron ions to the root of nanowires and lastly to the tip of nanowires (Yuan et al., 2012).	41
Figure 2.21	Schematic diagram of Fe Fe is supplied from the iron substrate and O <sub>2</sub> from the surroundings. Insets show rhombohedral tip and amorphous edge of the wires, which provide some hints on the growth mechanism (Hiralal et al., 2008).	41
Figure 2.22	Oxidation of iron at 650-750oC in presence of water vapour condition (Yuan et al., 2013).	43
Figure 3.1	Summary flowchart of this project.	44
Figure 3.2	Iron wire after cutting, grinding and ultrasonic cleaning.	46
Figure 3.3	Heating profile for formation of iron oxide.	46
Figure 3.4	Thermal oxidation of sample in water vapour using ultrasonic nebuliser.	48
Figure 3.5	Experimental setup for photocatalysis process.	53
Figure 3.6	Diluted solutions for calibration purpose.	54
Figure 3.7	Calibration curve for Cr(VI) standard solutions.	54
Figure 4.1	Physical appearance of oxidised iron wire at 400 °C to 700 °C (all samples were oxidised in water vapour atmosphere) for an hour.	56
Figure 4.2	FESEM images of iron wires oxidised at (a and b) 400 °C, (c and d) 500 °C, (e and f) 600 °C and (g and h) 700 °C in dry air and water vapour atmosphere.	59

Figure 4.3	TEM image of nanostructure formed by iron wire oxidised at 600 °C (in water vapour). Insets show the corresponding lattice spacings.	60
Figure 4.4	Raman shift of oxidised iron wires at (a) 400 °C, (b) 500 °C, (c) 600 °C and (d) 700 °C.	61
Figure 4.5	Overview of FESEM image of oxidised iron wires at 500 °C in water vapour for (a) 15 minutes, (b) 30 minutes and (c) 60 minutes.	63
Figure 4.6	FESEM images of oxidised iron wire at 500 °C in water vapour for (a and b) 15, (c and d) 30 and (e and f) 60 minutes.	66
Figure 4.7	Schematic diagram of the cross-sectional view of iron wire and the structures formed at different oxidation time.	66
Figure 4.8	Physical appearance of iron foils oxidised at 500 °C and 700 °C for 1 hour.	67
Figure 4.9	FESEM images of iron foils oxidised at (a and b) 500 °C and (c and d) 700 °C.	69
Figure 4.10	FESEM images of iron foils oxidised at (a and b) 500 °C and (c and d) 700 °C. The samples were 45° tilted.	69
Figure 4.11	XRD diffraction pattern of iron foils oxidised at (a) 500 °C and (b) 700 °C.	70
Figure 4.12	Chemisorption of oxygen ions on iron wire substrate.	71
Figure 4.13	Phase diagram of iron-oxygen (Birks et al., 2006).	73
Figure 4.14	Cross section view of oxidised iron wire at 700 °C in presence of water vapour.	74
Figure 4.15	Cross-section view of oxidised iron wire at 700 °C in presence of water vapour.	75
Figure 4.16	Oxidation process of iron in water vapour.	75
Figure 4.17	Schematic diagram of stress induced during oxidation of iron wire.	76
Figure 4.18	Lateral growth of nanowire and merging of nanowire together.	79
Figure 4.19	Merging of anosheets to form porous structure.	79
Figure 4.20	Band energy levels for several chosen semiconductor oxides against the standard electrochemical potential scale (SHE) and the vacuum energy scale (Xu and Schoonen, 2000).	81
Figure 4.21	Schematic illustration of photoreduction of Cr(VI) under sunlight.	82

Figure 4.22	(a) Schematic illustration, (b) real image of Cr(VI) solution in the presence of photocatalyst sample and (c) the experimental setup for photocatalytic experiment.	83
Figure 4.23	Cr(VI) after DPC treatment.	83
Figure 4.24	Photoreduction of Cr(VI) in solution at pH (a) 5 and (b) 2 under sunlight irradiation.	86
Figure 4.25	Reduction percentage of Cr(VI) in solution at pH (a) 5 and (b) 2.	86
Figure 4.26	Surface protonated of iron oxide at pH (a) 5 and (b) 2.	87
Figure 4.27	Photoreduction of Cr(VI) in solution (a) without photocatalyst and in the presence of iron wire (1 cm long) oxidised at (b) 400 °C, (c) 500 °C, (d (i)) sample oxidised at 600 °C, (d (ii)) repeated experiment of sample oxidised at 600 °C and (e) 700 °C	88
Figure 4.28	Reduction percentage of Cr(VI) in solution (a) without photocatalyst and in the presence of iron wire (1 cm long) oxidised at (b) 400 °C, (c) 500 °C, (d) (d (i)) sample oxidised at 600 °C, (d (ii)) repeated experiment of sample oxidised at 600 °C and and (e) 700 °C.	89
Figure 4.29	FESEM images of iron wire oxidised at (a) 400 °C, (b) 500 °C, (d) 600 °C and (d) 700 °C.	89
Figure 4.30	Graphical illustration of sample oxidised at 700 °C. The inset is the EDX result of sample.	91
Figure 4.31	Photocatalytic reduction of Cr(VI) using photocatalyst of sample oxidised for (a) 15 minutes, (b) 30 minutes and (c) 60 minutes.	94
Figure 4.32	Reduction percentage of Cr(VI) in solution using photocatalyst of sample oxidised for (a) 15 minutes, (b) 30 minutes and (c) 60 minutes.	95

## LIST OF ABBREVIATIONS

0 – D	Zero Dimensional
1 – D	One Dimensional
2 – D	Two Dimensional
3 – D	Three Dimensional
<i>et al</i>	et al
DPC	Diphenyl-carbazide
EDX	Energy Dispersive X-ray
FESEM	Field Emission Scanning Electron Microscope
SEM	Scanning Electron Microscope
HRTEM	High Resolution Transmission Electron Microscope
XRD	X-Ray Diffraction
IARC	International Agency for Research on Cancer
ICSD	Inorganic Crystal Structure Database

## LIST OF SYMBOLS

Fe	Iron
FeO	Wustite
Fe <sub>3</sub> O <sub>4</sub>	Magnetite
$\alpha$ -Fe <sub>2</sub> O <sub>3</sub>	Hematite
$\gamma$ -Fe <sub>2</sub> O <sub>3</sub>	Maghemite
at %	Atomic percent
wt %	Weight percent
°C	Degree Celsius
°C/min	Degree Celsius per Minute
ppm	Part per million
Cr (VI)	Hexavalent Chromium
Cr (III)	Trivalent Chromium
Fe <sup>2+</sup>	Iron (II) Ion
Fe <sup>3+</sup>	Iron (III) Ion
OH <sup>-</sup>	Hydroxide Ion
ml	milliliter
Å	Angstrom
nm	nanometer
μm	micrometer
TiO <sub>2</sub>	Titanium Oxide
min	Minute

# **PEMBENTUKAN BESI OKSIDA STRUKTUR BERLIANG HIERARKI DAN APLIKASI MEREKA DALAM PENGURANGAN Cr(VI)**

## **ABSTRAK**

Cr(VI) adalah logam berat yang toksik dan telah diklasifikasikan sebagai karsinogenik kepada manusia. Cr(VI) memasuki ke alam sekitar daripada sumber seperti aloi dan pembuatan keluli, dan industri pembuatan getah.. Kajian ini menyiasat aplikasi oksida besi berliang hierarki dalam penyingkiran Cr(VI). Besi oksida struktur berliang hierarki telah disintesis oleh pengoksidaan langsung dawai besi dalam suasana wap air. Besi oksida yang disintesis telah disifatkan dan dicirikan oleh Mikroskop Elektron Pengimbas Pancaran Medan (FESEM), Microskop Elektron Transmisi Resolusi Tinggi (HRTEM) dan Raman. Parameter pengoksidaan yang telah dikaji adalah kesan suhu pengoksidaan, masa pengoksidaan dan kewujudan wap air semasa pembentukan. Pengoksidaan pada suhu yang berbeza telah menghasilkan wayar nano pada 400 °C, kepingan nano pada 500 °C, struktur berliang hierarki pada 600 °C and kepingan oksida pada 700 °C. Struktur berliang hierarki telah dihasilkan apabila pengoksidaan dijalankan dalam suasana wap air pada 400 °C to 600 °C dan kepingan oksida dihasilkan pada 700 °C dalam suasana wap air. Jangka masa untuk menghasilkan struktur nano pada 500 °C telah dikaji Didapati bahawa campuran wayar nano dengan kepingan nano dibentuk dalam masa 15 minit pengoksidaan dan kepingan nano dibentuk banyak dengan campuran dalam masa 30 minute pengoksidaan. Struktur berliang hierarki mengambil masa satu jam untuk terhasil. Mekanisma untuk penghasilan struktur nano pada permukaan besi telah dicadang mengikut dorongan tekanan. Struktur berliang hierarki terhasil apabila kepingan nano bertumbuh and dinding mereka bertemu. Peratusan pengurangan untuk Cr(VI) pada pH 2 adalah paling tinggi untuk sampel oksida pada suhu

500 °C dan satu jam (59.09 %) berbanding dengan sampel oksida selama 30 minit (54.54 %) dan 15 minit (38.64 %).

# **FORMATION OF HIERARCHICAL POROUS IRON OXIDE AND THEIR APPLICATION IN REDUCING Cr(VI)**

## **ABSTRACT**

Cr(VI) is heavy metal of high toxicity and has been classified as human carcinogen. Cr(VI) enters into environment from sources such as leather and tanning, alloys and steel manufacturing and rubber manufacturing industries. This study investigated the applicability of hierarchical porous iron oxide for the removal of Cr(VI) from aqueous solution. The hierarchical porous structures were synthesized by direct thermal oxidation of iron wire in water vapour atmosphere. The synthesized hierarchical porous iron oxide were characterized by Field Emission Scanning Electron Microscope (FESEM), High Resolution Transmission Electron Microscope (HRTEM) and Raman spectroscopy. Oxidation parameters investigated were the effect of oxidation temperature, time and presence of water vapour. Oxidation at different temperatures resulted in the formation of nanowires at 400 °C, nanosheets at 500 °C, hierarchical porous structure at 600 °C and blades formed at 700 °C. Hierarchical porous structure formed when oxidation carried out in water vapour for 400 °C to 600 °C and blades structures was formed at 700 °C in water vapour. Different oxidation time at 500 °C in water vapour was conducted to investigate the growth of nanostructures on iron wire. A mixture of nanowires and blades formed at 15 min of oxidation time and more blades formed with few nanowires after 30 min. Hierarchical porous structures were observed after 1 hour oxidation. The growth of nanostructures on iron oxide was suggested to follow the stress-driven mechanism. The longer oxidation time leads to lateral growth of nanowires which then turn to blade structure and hierarchical structures formed when the walls of blade meet. The reduction percentage of Cr(VI) at pH 2 is the highest for sample oxidised at 500 °C for 1 hour

(59.09 %) compared to the one at 30 minutes (58.55 %) and 15 minutes (38.64 %), respectively.

# CHAPTER 1

## INTRODUCTION

In this project, thermal oxidation of iron wires was done to form surface oxide comprising of iron oxide with nanostructures. The nanostructures were found to be in a form of hierarchical porous nanostructure as well as thin sheets or blades and nanowires. The iron oxide nanostructures produced were then used as photocatalysts to reduce hexavalent chromium (Cr(VI)) to trivalent chromium (Cr(III)) under solar irradiation. This chapter is on the background, problem statements, objectives, scopes of work and outline of the report.

### 1.1 Background

Even though water is considered abundant on earth; only a small fraction is readily available and safe for human consumption. This is because water is polluted due to urbanisation, population growth and development of industrialisation (Chong et al., 2010). Water pollution affects all the major water bodies of the world such as rivers, groundwater and marine water. Pollution creates further problems: contamination of marine life and soil which then polluting fish and crops respectively. Upon consumption, human will also be affected by the pollutants. Polluted water is not only unfitted for drinking but also for other uses such as domestic, agriculture and industrial applications.

In Johor, for example, fourteen rivers were reported in 2008 to have moderate pollution levels while five rivers in the Tebrau catchment had more severe pollution (Grafton et al., 2015). Industrial and development activities have caused severe pollution of the river in Pasir Gudang, Johor catchment (Ewing, 2016). Based on Water Environment Partnership in Asia (WEPA), in 5,613 water samples that were being analysed, almost all samples complied with Class III, National Water Quality Standards

for arsenic (As), cadmium (Cd), chromium (Cr), mercury (Hg), lead (Pb) and zinc (Zn), except iron (Fe) with 83 percent compliance (Chakraborty and Mukhopadhyay, 2014). This is to say that, heavy metal ions listed above are existed in most of the rivers in Malaysia which is undesirable for consumption or other purpose.

There are many different types of pollutants in water, but heavy metal ions is one of the most severe. These heavy metals are harmful to human beings and ecological environment. For example, extensive use of chromium compounds in industrial applications has resulted in massive amounts of wastewater containing toxic chromium species. Therefore, the need of removal of heavy metals has become a must and many was have been proposed by researchers. In this project, nanomaterials were synthesised as to remove hexavalent chromium (Cr(VI)) ions via photocatalytic reduction process.

## **1.2 Removal of Cr(VI) from Water Bodies**

Chromium, discovered by Nicholas Louis Vauquelin, is classified as one of the heavy metal elements on earth. Chromium enters into the environment from various sources and is commonly used in the leather and tanning industries, alloys and steel manufacturing and rubber manufacturing applications (Gautam et al., 2014). Chromium in oxidation state +3 is considered essential for good health in moderate intake, however, chromium in oxidation state +6 is considered harmful even in small intake quantity (Guertin et al., 2004). Hexavalent chromium, Cr(VI), is the second most stable oxidation state of chromium and has been categorised as Group 1 materials which is human carcinogen by International Agency for Research on Cancer (IARC). Excessive exposure to Cr(VI) can cause severe health problems such as skin ulceration, damage of liver and kidney and even to the central nerve system (Sharma, 2014).

According to World Health Organization (WHO) International Standards for Drinking-water, the maximum allowable concentration of Cr(VI) is 0.05 mg/litre (WHO, 2004). In the United States, the EPA under the authority of the Safe Drinking Water Act (SDWA) has set the Maximum Contaminant Level (MCL) and the Maximum Contaminant Level Goal (MCLG) for chromium at 0.10 mg/litre while in Malaysia, parameter limits of effluent of Cr(VI) is 0.05 mg/litre based on Environmental Quality Act, 1974 and the Malaysia Environmental Quality (Sewage and Industrial Effluents) Regulations, 1979, 1999, 2000. However, disposal of Cr(VI) to our water from industrial processes sometimes exceeds the value. Therefore, methods to reduce or eliminate the discharge of Cr(VI) to water bodies are required.

Various methods have been employed to remove Cr(VI) from wastewater or polluted water such as ion exchange (Rafati et al., 2010), electrochemical treatment (Rodriguez et al., 2003), chemical precipitation (Ramakrishnaiah and Prathima, 2012), membrane filtration (Gunatilake, 2015), adsorption (Burks et al., 2014) and photocatalytic technology (Barrera-Díaz et al., 2012, Li et al., 2017, Chen et al., 2017). Among these techniques, photocatalytic technology has caught attention by offering benefits which includes low cost, cleanliness, ease of operation and high efficiency.

Since 1970s, photocatalytic technology has been studied and widely explored. It is especially beneficial for the transformation of toxic material to less dangerous product in the presence of a solid catalysts which can only be activated under light irradiation. Reactive electrons and holes generated on the surface of semiconductor formed under light irradiation with energy greater than the semiconductor bandgap energy can be used for catalytic processes (Ghorab et al., 2013). Electrons from the valence band will be excited to the conduction band, and holes will be generated in the valence band as shown in Figure 1.1. These electrons and holes either recombine or become involved in reduction

and oxidation reactions. It has been reported that the application of photocatalytic reduction can efficiently remove many heavy metal ions, like  $\text{Ag}^+$ ,  $\text{Cu(II)}$ ,  $\text{Hg(II)}$  and  $\text{Cr(VI)}$  (Khalil et al., 1998, Kabra et al., 2004, Ch et al., 2008).

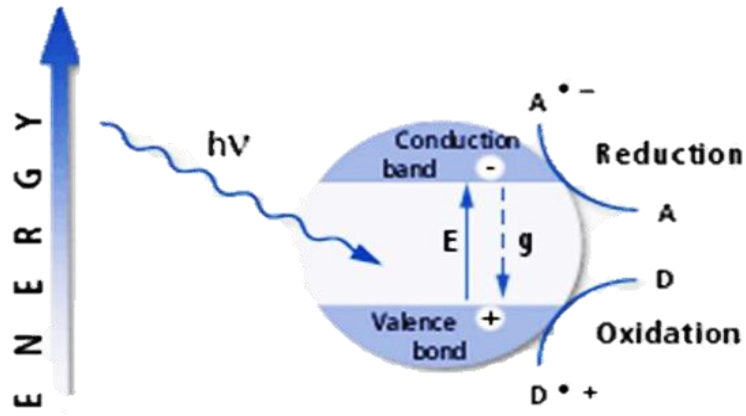


Figure 1.1: Photocatalysis on a semiconductor (Philippopoulos and Nikolaki, 2010).

Metal oxide semiconductor photocatalysts are of interest due to their applications in environmental pollution control purpose in which they use their photocatalytic reduction capability in removing heavy metal. The use of titanium oxide ( $\text{TiO}_2$ ) as photocatalyst has been most extensive due to its photoactivity, low cost and stability (Shon et al., 2008). However, the use of  $\text{TiO}_2$  as photocatalyst in wastewater treatment is limited.  $\text{TiO}_2$  has a weak response towards visible light due to it has wide bandgap energy, 3.2 eV. Therefore, the energy source in  $\text{TiO}_2$  is limited to UV or near UV radiation as  $\text{TiO}_2$  can be triggered by radiation source with wavelength of less than 380nm. Iron oxide, on the other hand, is an n-type semiconductor with narrow bandgap of 2.2eV which can be a good photocatalyst absorbing visible light. Also, abundance and environmental friendliness are some of the advantages of iron oxides. As iron oxide has certain magnetoc properties, the oxide can be easil removed from treated water by a magnet or external magnetic field. This can reduce secondary pollution. Iron oxide can be formed by various

processes. In this project a simple oxidation process was done by heating up iron wire. The oxidised iron was then used to reduce Cr(VI).

Iron, with chemical symbol “Fe”, is one of the most common metals that normally found on earth’s crust as iron ore or meteorites (Hasan, 2004) which contributes to its ease of availability. Iron has 16 kinds of oxides and oxide-hydroxides (Cornell and Schwertmann, 2006). Its oxides, containing Fe with O and/or OH, are easily produced in the laboratory and also extensively spread in nature. Iron oxides that exist in nature can occur in various compartment of the global system as shown in Figure 1.2.

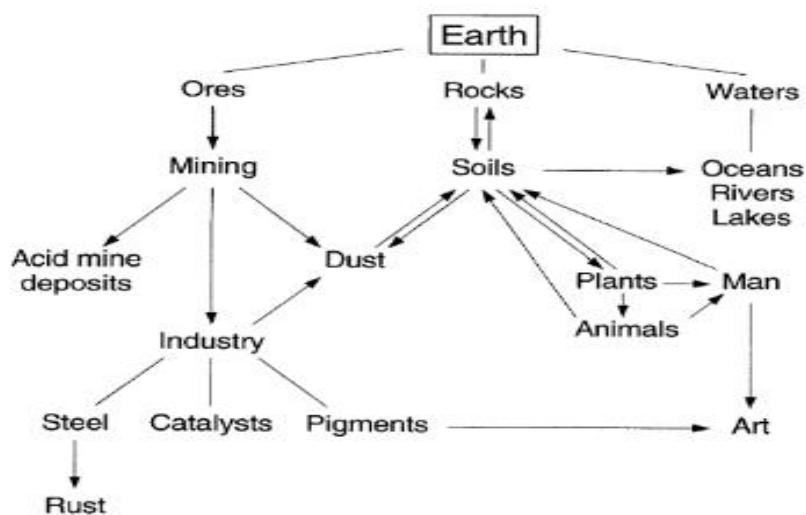


Figure 1.2: Iron oxides in the global system (Cornell and Schwertmann, 2006).

Figure 1.3 shows the six most important oxides of iron. However, iron oxide normally exists in three common forms: hematite ( $\alpha\text{-Fe}_2\text{O}_3$ ), maghemite ( $\gamma\text{-Fe}_2\text{O}_3$ ) and magnetite ( $\text{Fe}_3\text{O}_4$ ) (Xu et al., 2012). There have been a number of investigations on the application of iron oxides on chromium (VI) removal such as flowerlike  $\alpha\text{-Fe}_2\text{O}_3$  (Zhong et al., 2006),  $\text{Fe@Fe}_2\text{O}_3$  core-shell nanowires (Ai et al., 2008) and iron (III)-based metal-organic frameworks (Shi et al., 2015). The use of nanoscale materials has been suggested for wastewater treatment due to their efficiency and cost effectiveness (Xu et al., 2012). Hematite ( $\alpha\text{-Fe}_2\text{O}_3$ ), the first known iron oxide, is extremely stable compared to other

phase of iron oxides and it is usually the end member of transformation of other iron oxides (Cornell and Schwertmann, 2006). Same as its bulk material, nanostructured  $\alpha$ - $\text{Fe}_2\text{O}_3$  has been applied to wide range of applications such as electrode materials, gas sensor (Chen et al., 2005), catalyst (Han et al., 2006), water splitting (Gao et al., 2011) and magnetic recording media (Yuan et al., 2012).

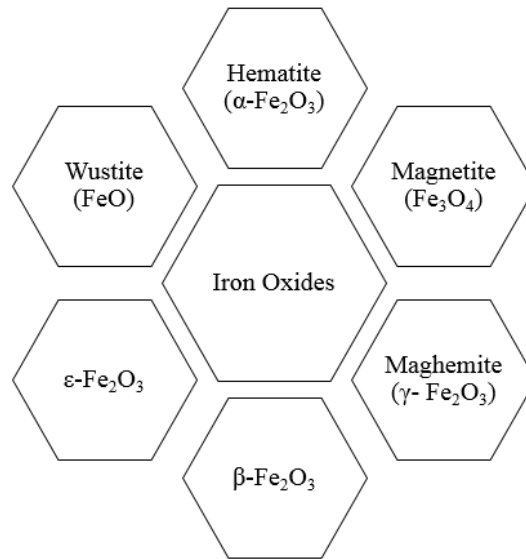


Figure 1.3: Types of iron oxides.

### 1.3 Nanomaterials

Nanomaterial is commonly referred as a material with structure of size ranging from 1 to 100nm at least in one dimension (Xu et al., 2012). Nanomaterial possesses properties that are not found in its bulk-sized counterpart material. It is expected that iron oxide in nanoscale structure would improve the photocatalysis performance when more surface area is generated. Nanomaterials are not new undiscovered material but it can be metal, polymer, ceramics or semiconductor material with dimensions in nanoscale. Nanomaterials can be classified into four categories according to the number of dimensions which are not restricted to the nanoscale range: zero-dimensional (0-D), one-dimensional (1-D), two-dimensional (2-D) and three-dimensional (3-D) as shown in

Figure 1.4. 3-D nanostructures have caught much interest due to their unique properties of combining other classes of nanomaterials into a larger system or device to form a so-called “bulk nanomaterials”. Here, 1 cm of 0.5 mm iron wire was oxidised to form nanosheets or blades with thickness < 50 nm. Such 3-D system has an advantage of ease of handling and once used it can be removed easily without introducing secondary pollution.

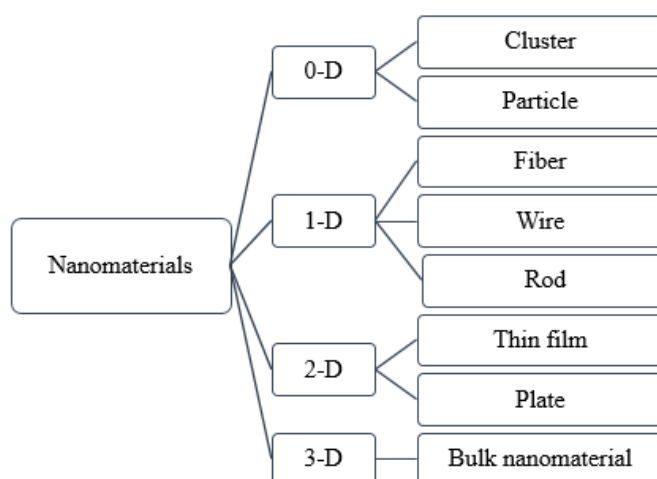


Figure 1.4: Classification of nanomaterials.

Undoubtedly, there has been a vigorous growth of nanoscience especially on the technique to synthesise or fabricate nanostructured materials in the past few years as well as on the characterizations of them.

#### 1.4 Iron Oxide as Photocatalysts

Different types of nanosized metal oxides such as titanium oxides as mentioned before, ferric oxides, aluminium oxides, manganese oxides and cerium oxides are capable of heavy metal removal from wastewater (Hu et al., 2005, Hua et al., 2012). Iron oxide was selected, as mentioned due to its narrow energy gap. Moreover, their efficiency to reduce heavy metal that contributed by its small size (in nano range) and high surface to volume ratio can be enhanced by synthesising the oxide in the nanoscale. Besides, the use

of nanostructured iron oxide is beneficial for wastewater treatment due to their availability, ease of separation, low cost, low toxicity and enhanced stability (Xu et al., 2012). The growth of oxide on metal substrate can be done by oxidation of the substrate. Such structure is considered to be more robust as it is adhered to rigid body. Therefore after photocatalytic Cr(VI) removal process is completed, the oxidised wire can be easily removed from the treated water. Furthermore, as iron is environmentally friendly, the risk for secondary contamination is minimized as well. Also, it is noted that with the presence of iron as a reducing agent, Cr(III) will be formed by the reduction of Cr(VI) (IARC, 2012). This project, as mentioned, focus on the formation of nanostructured iron oxides and also on assessing their application in Cr(VI) removal.

Different approaches have been studied to synthesize nanostructure iron oxide such as the template method, metal–organic chemical vapor deposition (Cha et al., 2009), sol-gel deposition (Woo et al., 2003), hydrothermal (Tang et al., 2006, Almeida et al., 2009) and thermal oxidation (Hiralal et al., 2008, Yuan et al., 2012, Budiman et al., 2016). Nevertheless, the assembly of the low dimensional building blocks (particles, wires, tubes and flakes) into a complex 3-D nanostructures is considerably more challenging. Thermal oxidation method was used in this project to produce nanostructure iron oxide as it is a direct, simple and inexpensive (Vincent et al., 2012). Thermal oxidation is also a rather rapid process compared to other methods. The oxide layer is formed on the metal surface under elevated temperature and oxidising condition. As mentioned, this project was targeted to produce nanostructure iron oxide as photocatalyst for Cr(VI) reduction from wastewater. Hierarchical porous iron oxide comprising of nanosheets or blades were grown on the iron wire form by heating the iron wire in a furnace. The effects of oxidation temperature, time and atmosphere were observed and the use of iron oxide nanowires as photocatalyst was explored as well.

## 1.5 Problem Statement

Water pollution is increasing globally resulted in the growth of population and industry (Dave and Chopda, 2014). Even a trace amount of heavy metal present in water resources could be detrimental to human being. Heavy metal pollution creates serious problem to both human being and environmental system which makes the removal of heavy metal so necessary. The use of nanostructured iron oxide for removal of heavy metals contamination from wastewater has caught much attention due to their outstanding features. Various method either physical, biological or chemical method have been conducted to synthesise and investigate the morphology of different nanostructure of iron oxide especially in particle form: nanoparticles, nanowires, nanobelts, nanofibers, and nanotubes. However, photocatalysts in powdered possess a problem of agglomeration and are difficult to be separated from the treated water. Also, there are no available information on the assessment of the use of hierarchical structure for Cr(VI) removal. In this project, hierarchical porous iron oxide was synthesised by thermal oxidation through quenching process, and by this, the problems related to agglomeration in solution and secondary pollutions by the photocatalyst can be prevented as the nanostructures are supported by a substrate.

The synthesis of iron oxide with nanowires structure was reported by Takagi (1957) despite the structure was termed “whiskers”. Takagi reported on the formation of  $\alpha$ -Fe<sub>2</sub>O<sub>3</sub> whiskers on pure iron in oxygen atmosphere at different temperatures. Following Takagi several works have been reported on the formation of such whiskers. The whiskers are also grown laterally to form blades as mentioned by Voss et al (1982). It was not until in 2000 that the term nanowires was used to describe the whiskers and nanosheets to describe blades. For instance, Fu et al (2001) reported that hematite “nanowires” can be synthesised by heating pure iron foil in an oxidizing mixture atmosphere consisting of

CO<sub>2</sub>, N<sub>2</sub>, SO<sub>2</sub> and H<sub>2</sub>O. The synthesis of iron oxide nanostructures depends on parameters such as oxidation temperature, time, pressure and atmosphere. The increase of time and temperature have been reported to increase the size and density of iron oxide nanowires. However, long oxidation time is usually required to form dense nanowires (Srivastava et al., 2007). Many efforts have been made after them to improve the method by reducing the oxidation time and the complexity of the mixture of gases used. A rapid way for synthesis of nanowires can be reached by direct plasma oxidation on bulk material (Cvelbar et al., 2008), but this approach is complicated as it needs the precise control of plasma creation. On the other hand, it is reported that most hierarchically structured iron oxides can be formed by employing template methods. Zhong et al. (2006) reported the formation of flowerlike hierarchical iron oxide structure through soft template method by tetrabutylammonium bromide (TBAB) via two steps process. Hard template was employed by Yuan et al. (2006) by using activated carbon fibers as the template to produce hierarchical structures of metal oxides. However, there is less information for the photocatalytic reduction ability of hierarchical porous structure iron oxide. Therefore, in this project, (i) hierarchical structure was produced by oxidation via quenching process then (ii) the photocatalytic reduction performance of hierarchical porous structures formed was presented.

Another modification done in this project was oxidation in water vapour. According to Young (2016), the corrosion rate can be accelerated when iron and steel material are oxidised in atmosphere containing water vapour. Yuan et al (2013) show that presence of water vapour enhances the oxidation rate. In this work, thermal oxidation of iron was done in the presence of water vapour in order to produce more densely packed nanostructure on the iron substrate. The mechanism of oxide growth in the presence of

water at high temperature was studied. No other work is found to report on the formation of nanostructures under water vapour via rapid quenching processes.

## **1.6 Objectives**

The main objectives of this research work are:

1. To investigate the morphologies of oxide on high purity iron wire by quenching process in thermal oxidation.
2. To study the effect of water vapour during oxidation process on the morphologies of iron oxide.
3. To assess the photocatalytic removal properties of iron oxide nanostructures on Cr(VI) removal.

## **1.7 Scopes of Work**

This project covered the investigation on the formation of iron oxide nanostructures and their ability on Cr(VI) photocatalytic reduction to reduce Cr(VI) to Cr(III). Thermal oxidation process was selected for the synthesis of iron oxide nanostructures. For thermal oxidation process, the effect of temperature, oxidation atmosphere and time were studied. High purity iron wire was used in this research. Phase and morphology characterization of the nanostructure iron oxide was determined by X-Ray Diffraction (XRD), Raman spectroscopy, Transmission Electron Microscope (TEM) and Field Emission Scanning Electron Microscopy (FESEM).

## **1.8 Outline of Chapters**

This thesis consists of five chapters. Chapter one discusses on the introduction, objectives, research motivation, problem statement and study scopes of the project. Meanwhile, the concept, theory and literature review related to the fabrication of iron oxide nanostructures by using thermal oxidation method are explained in chapter two. In chapter three, experimental details and characterization approaches are explained

respectively. While chapter four focuses on presenting the results and discussion of this project. Finally, conclusion of this project and recommendations of future work are stated in chapter five.

## CHAPTER 2

### LITERATURE REVIEW

#### 2.1 Introduction

This project is on the formation of hierarchical porous iron oxide as photocatalyst by thermal oxidation of iron wire for the removal of hexavalent chromium. This chapter focuses on the problems of chromium as heavy metal ions pollutant in the environment. Then approaches to remove hexavalent chromium are reviewed. The later part of this chapter describes iron oxide as the material chosen and its general properties as well as the formation process.

#### 2.2 Basics of Chromium

Chromium, discovered in 1797, by French chemist Nicola-Louis Vauquelin has its name originated from Greek word *chroma* which means colour as its compounds exist in various colours. It is a silver-grey metal that able to be polished until shiny. It is the twenty-fourth element in the periodic table and is categorized as one of the heavy metals. Chromium is more abundant than metals such as gold, cobalt and molybdenum. Table 2.1 presents the properties of chromium.

Table 2.1: General properties of chromium (Lepora, 2005).

PROPERTIES	CHROMIUM
Chemical Symbol	Cr
Atomic Number	24
Atomic Mass	52
Melting Point	1907°C (3375°F)
Boiling Point	2671°C (4842°F)
Density	7.14g/cm <sup>3</sup>

Chromium exists in oxidation states range from -2 to +6. The common forms of chromium are  $\text{Cr}^0$ ,  $\text{Cr}^{+2}$ ,  $\text{Cr}^{+3}$  and  $\text{Cr}^{+6}$ . However, only trivalent and hexavalent chromium are found in nature because divalent chromium is not a stable form and will oxidize to trivalent state. Chromium, in its hexavalent state, is a strong oxidizing agent which usually found in the forms of chromate ( $\text{CrO}_4^{2-}$ ) or dichromate ( $\text{Cr}_2\text{O}_7^{2-}$ ) (National Research Council Committee on Biologic Effects of Atmospheric Pollutants, 1974). Cr(VI) shows carcinogenic property and Cr(III) is essential to maintain the normal level of glucose in human (Mandina and Mugadza, 2013).

As seen from Figure 2.1, the dominating species of trivalent chromium are  $\text{CrOH}^{2+}$ ,  $\text{Cr(OH)}_2^+$  and  $\text{Cr(OH)}_3$  at the pH range of 4 to 10 while the expected forms of hexavalent chromium in natural water are  $\text{CrO}_4^{2-}$ ,  $\text{HCrO}_4^-$  and  $\text{Cr}_2\text{O}_7^{2-}$  (Kotaš and Stasicka, 2000). Cr(VI) species also depends on pH where the predominant form at the pH range from 1 to 6 is  $\text{HCrO}_4^-$  and  $\text{CrO}_4^{2-}$  for pH above 7. Cr(VI) is therefore quite mobile in the environment due to many of Cr(VI) compounds are more soluble than that of Cr(III).

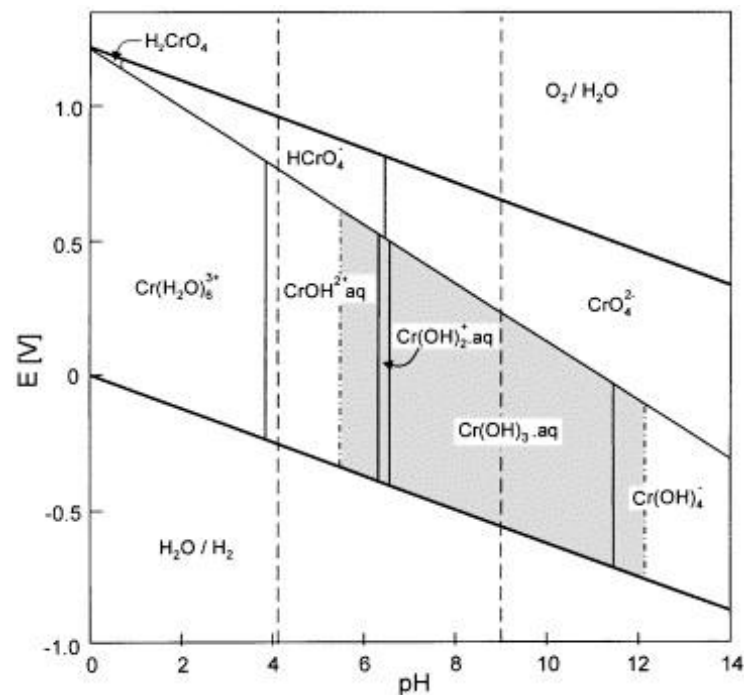


Figure 2.1: Pourbaix diagram for chromium species (Kotaš and Stasicka, 2000).

### **2.3 Chromium in Nutrition and Its Effect to Human**

Chromium is being accepted as an essential element for human. Deficiency of chromium causes cardiovascular disease, increase of body fat, elevated circulating insulin and impaired glucose tolerance. The daily minimum intake for chromium is estimated to be 33 $\mu$ g per person to meet normal requirement (WHO, 1996). Chromium normally occurs in the environment in two forms which are Cr(III) and Cr(VI). Chromium in metal form is biologically inert and does not produce chronic effects to human (National Research Council (U.S.). Committee on Biologic Effects of Atmospheric Pollutants, 1974). Chromium in its trivalent state is an essential nutrient for human in trace amount but hexavalent chromium is toxic.

Metallic chromium and trivalent chromium were classified in Group 3 by IARC because they were not classifiable as to their carcinogenicity to humans (IARC, 2012). However, hexavalent chromium is hazardous especially through inhalation by lung and gastrointestinal tract, or even through the contact with skin. Inhaled hexavalent chromium has been classified as human carcinogen by the United States Environmental Protection Agency and the International Agency for Research on Cancer (Grevatt, 1998, IARC, 2012). Besides, genotoxic effects like chromosomal aberrations or sister chromatid exchanges in workers exposed to hexavalent chromium have been reported in studies on occupational exposure. Excess risk of lung cancer is also related to occupational exposure to hexavalent chromium (Gibb et al., 2000). As hexavalent chromium is highly toxic and carcinogen to living properties, and thus WHO has stated the allowable limit in drinking water for hexavalent chromium is 0.05mg/L (WHO, 2004).

### **2.4 Remediation of Cr(VI)**

Numerous techniques have been established for treating hexavalent chromium from wastewater. The techniques include ion exchange, chemical precipitation,

electrochemical treatment, membrane filtration and photocatalytic technology. The techniques include their advantages and disadvantages will be explained in the following subchapter.

### 2.3.1 Ion Exchange

Ion exchange is a physical process where ions in a solution are exchanged with other similarly charged ions in the presence of ion exchangers as shown in Figure 2.2. Ion exchangers can be synthetic resin, zeolites or clay. There are anion and cation exchangers. Anion exchangers exchange negatively charged ions while cation exchangers exchange positively charged ions. Anion exchanger resin is used for removal of Cr(VI) and the resin will bind the dissolved Cr(VI) ions as water to be treated flows through. The bound ions will then be displaced by the Cr(VI) ions (Guertin et al., 2004). The advantages of ion exchange method are the regeneration of the sorbent, reduction of chemical or biological sludge produced and the metal recovery possibility (Balan et al., 2013).

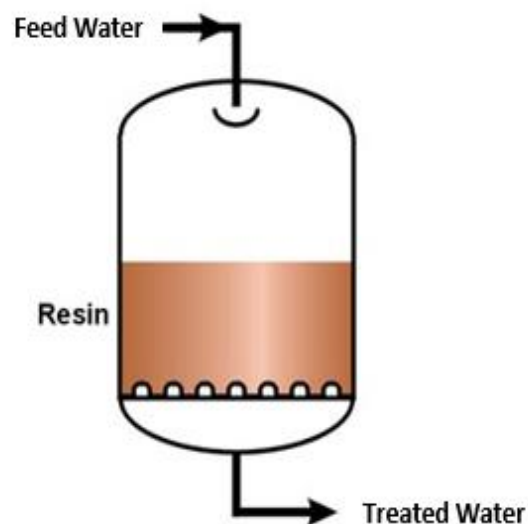


Figure 2.2: Schematic illustration of ion exchange process.

### 2.3.2 Chemical Precipitation

Chemical precipitation is the most traditionally used technique for the removal of hexavalent chromium to Cr(III) hydroxide (precipitate) by the addition of precipitant (Kaprra et al., 2013). It involves the separation of insoluble substance from a solution by converting the soluble substance into insoluble form. For the removal of chromium, the hexavalent chromium is first reduced to trivalent chromium and then followed by its precipitation to hydroxyl species (Barrera-Díaz et al., 2012). The common chemicals added for the precipitation are lime, ferrous sulphate and sulphur compounds. The use of lime as precipitant had resulted in the maximum precipitation of Cr(III) at pH 8.7 (Madhavi et al., 2013).

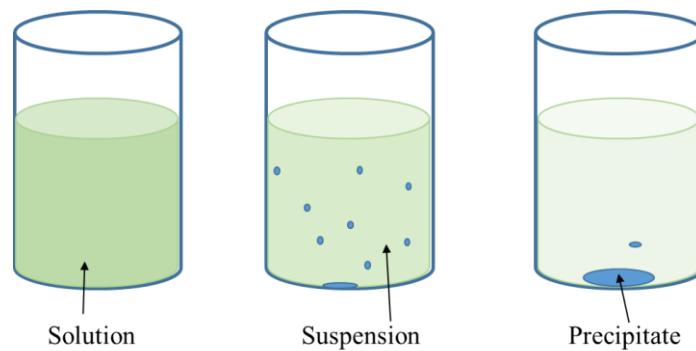


Figure 2.3: Schematic illustration of chemical precipitation method.

### 2.3.3 Electrochemical Treatment

Electrochemical treatment is the process of passing current through an electrolyte (aqueous metal-bearing solution) that contains cathode and anode as shown in Figure 2.4. Electrochemical treatment is one of the methods to treat wastewater. No chemical being added to the system and it is environmental friendly are the advantages of this method (Campos et al., 2007). However, it does not find wide application due to it is expensive method.

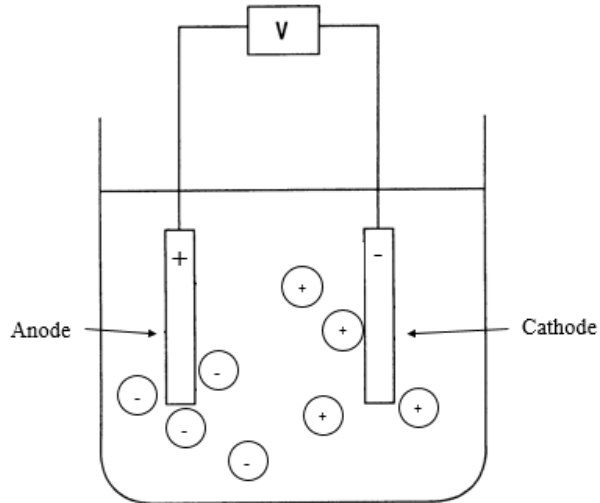


Figure 2. 4: Schematic illustration of electrochemical treatment process.

### 2.3.4 Membrane Filtration

Membrane filtration has also been used in treating wastewater. The water to be treated will be driven through a semi permeable membrane by pressure. The membrane acts as filter to catch unwanted compounds. Reverse osmosis, ultrafiltration and nanofiltration can be categorised to the types of membrane used in this method according to the size of the pore of membrane that can be separated by them (Kaprra et al., 2013). Examples of membranes are liquid emulsion membrane (Chiha et al., 2006), modified ultrafiltration carbon membrane (Pugazhenthii et al., 2005) and polymer enhanced ultrafiltration membrane (Aroua et al., 2007).

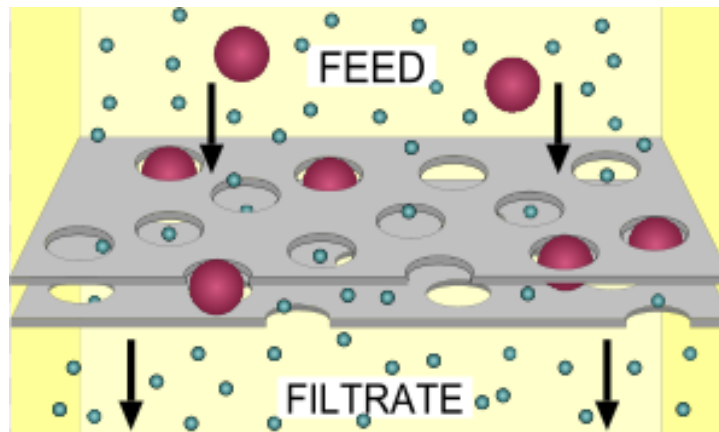


Figure 2. 5: Schematic diagram of membrane filtration technique.

### **2.3.5 Adsorption**

Adsorption is a method for heavy metal wastewater treatment due to its effectiveness and economic. Adsorption is the property of a material which is known as adsorbent that able to attract molecules or ions (adsorbate) (Budiman et al., 2016) which can happen through physical adsorption or chemical adsorption. Physical adsorption is referred to as phenomenon that Van der Waals forces occur between adsorbate and adsorbent whereas chemical adsorption is the attraction of molecule to a surface through chemical bond formation. The examples of adsorbents used are activated carbon, chitosan and fly ash. Various activated carbons were formed from wood, shells of coconut and dust coal to remove Cr(VI) (Madhavi et al., 2013).

### **2.3.6 Photocatalytic Technology**

Photocatalysis is method based on the reduction of Cr(VI) to Cr(III) on a semiconductor surface under light irradiation as illustrated in Figure 2.6. When the photon has energy equal or greater to the band gap of the semiconductor, electron- holes pair will be generated (Ghorab et al., 2013). Electrons and holes take part in the redox reaction and can react directly with adsorbed chromium ions. This method has large capability for removal trace amount of heavy metal. Visible light photocatalysis can be seen as a powerful tool in wastewater treatment due to its ease of use and attractive potential of applications. Semiconductor metal oxides have been studied as photocatalysts for the removal of Cr(VI). Among the semiconductors, TiO<sub>2</sub> is the most well-known, while others like ZnO, ZrO<sub>2</sub> and WO<sub>3</sub> have also gain much interest. Other non-oxide compound semiconductor like cadmium sulphide has also been used but CdS photocorrode and easily deactivated. Moreover cadmium is a rather toxic metal itself (Assadi et al., 2012). Iron oxides either hematite or magnetite are gaining much interest due to their ability to absorb and under illumination can reduced absorbed molecules on them. Moreover, iron

oxide has certain magnetic properties that can be applied for separation of the photocatalyst after application. Besides, hematite has a narrow bandgap ( $E_g=2.2\text{eV}$ ) allowing them to absorb visible light unlike  $\text{TiO}_2$  or  $\text{ZnO}$  with energy gap or  $> 3 \text{ eV}$  (Gandha et al., 2016). These oxides require UV lamp to generate photoelectrons. Ku et al. (2001) have reported on the reduction of  $\text{Cr(VI)}$  by  $\text{TiO}_2$  using fluorescent UV lamp as light source.

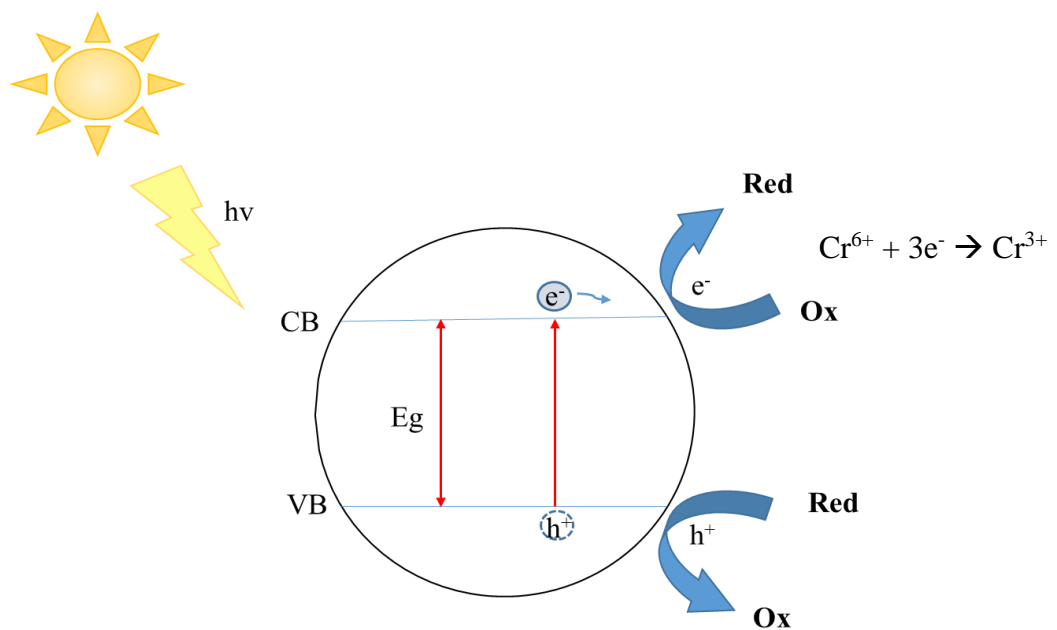


Figure 2.6: Photocatalysis under sunlight irradiation.

Several consideration should be taken into account to choose the best method for removal of  $\text{Cr(VI)}$  such as cost, efficiency, secondary pollutants and ease of operation (Xu et al., 2012). Table 2.2 presents the summary of the  $\text{Cr(VI)}$  treatment techniques. The advantages and disadvantages of the techniques are included in Table 2.2 as well. In this project, photocatalysis was chosen for  $\text{Cr(VI)}$  absorption and reduction via photogenerated electrons on iron oxide as photocatalysts.

Table 2.2: Comparison of Cr(VI) remediating techniques (Madhavi et al., 2013, Barrera-Díaz et al., 2012).

Remediating Techniques	Advantages	Disadvantages
<p>Ion exchange (Balan et al., 2013)</p> <p>Example: resin, zeolites and clay</p>	<ul style="list-style-type: none"> <li>✓ High removal efficiency</li> <li>✓ Fast process</li> <li>✓ Regeneration of the sorbent</li> <li>✓ Reduction of chemical or biological sludge</li> </ul>	<ul style="list-style-type: none"> <li>✗ Require regeneration of ion exchange resin</li> <li>✗ Require difference in affinity of ions in resin and ions to be removed</li> <li>✗ High operating cost</li> </ul>
<p>Chemical precipitation (Kaprrara et al., 2013)</p> <p>Example: lime and metal sulphides</p>	<ul style="list-style-type: none"> <li>✓ Operation is simple</li> <li>✓ Capital cost is low</li> </ul>	<ul style="list-style-type: none"> <li>✗ Ineffective in removal metal ions at low concentration</li> <li>✗ Generation of sludge leads to cost intensive disposal</li> <li>✗ Slow process</li> </ul>
<p>Membrane filtration (Kaprrara et al., 2013, Madhavi et al., 2013)</p> <p>Example: liquid emulsion membrane, modified ultra filtration carbon membrane</p>	<ul style="list-style-type: none"> <li>✓ Simple technique</li> <li>✓ Space saving</li> <li>✓ High efficiency</li> </ul>	<ul style="list-style-type: none"> <li>✗ High capital investment and high operational cost</li> <li>✗ Generation of sludge</li> <li>✗ Dependent on the size of the membrane</li> <li>✗ Selective removal; only molecules of certain size can be removed</li> </ul>
<p>Electrochemical (Kaprrara et al., 2013)</p> <p>Example: carbon aerogel electrode</p>	<ul style="list-style-type: none"> <li>✓ Fast process</li> <li>✓ Require fewer chemicals in the system</li> <li>✓ Less sludge produced</li> </ul>	<ul style="list-style-type: none"> <li>✗ Large capital investment</li> <li>✗ Expensive method</li> <li>✗ Chemical used can introduce another sort of pollutions</li> </ul>
<p>Adsorption (Budiman et al., 2016)</p> <p>Example: Chitosan and activated carbon</p>	<ul style="list-style-type: none"> <li>✓ Low cost</li> <li>✓ Ease of condition for operating</li> </ul>	<ul style="list-style-type: none"> <li>✗ Limited tolerant for pH range</li> <li>✗ Adsorption performance depends on type of adsorbent</li> <li>✗ Adsorption efficiency depends on production of waste products</li> </ul>
<p>Photocatalysis (Barrera-Díaz et al., 2012, Gandha et al., 2016)</p> <p>Example: TiO<sub>2</sub>, ZnO</p>	<ul style="list-style-type: none"> <li>✓ Low cost</li> <li>✓ Ease of operation</li> <li>✓ High efficiency</li> <li>✓ Cleanliness</li> </ul>	<ul style="list-style-type: none"> <li>✗ Depends on sunlight (intensity and irradiation) and weather</li> <li>✗ Depends on the energy gap of the semiconductor photocatalysts</li> <li>✗ Requiring additional source of light for activation</li> </ul>

### 2.3.7 Cr(VI) Removal by Iron Oxide

There have been several reports on the removal of Cr(VI) on iron oxides of varying phases: hematite –  $\alpha$ -Fe<sub>2</sub>O<sub>3</sub>, magnetite – Fe<sub>3</sub>O<sub>4</sub> and maghemite –  $\gamma$ -Fe<sub>2</sub>O<sub>3</sub>. Most of the reported works were focused on the synthesis of composite of iron oxide with another compound for the reduction of Cr(VI). This is because the compound formed able enhance the transport of photoexcited electrons by providing high surface area and also improvement in the separation of charge. A series of  $\alpha$ -Fe<sub>2</sub>O<sub>3</sub> with hydroxyl were studied by Wang et al. (2016) and the maximum of Cr(VI) reduction was 70.2% after one hour irradiation of light on Fe<sub>2</sub>O<sub>3</sub> sample produced in n-butyl alcohol.

Du et al. (2015) reported on a maximum Cr(VI) removal rate of 95.28% for  $\alpha$ -Fe<sub>2</sub>O<sub>3</sub> deposited on porous activated microwave expanded graphite oxide (aMEGO) and 25.26% for pure  $\alpha$ -Fe<sub>2</sub>O<sub>3</sub> while Zhang et al. (Zhang et al., 2016) have reported on formation of 3D blooming flower-like Fe<sub>2</sub>O<sub>3</sub>-MoS<sub>2</sub> nanocomposite which could reduce Cr(VI) thoroughly within 120 minutes of irradiation time. Also, it was found that the photoreduction of Cr(VI) is strongly affected by pH of the solution where the photocatalytic activity of the composite decreases with the increasing of pH of the solution (Padhi and Parida, 2014). The decrease of the photocatalytic activity is due to the surface of the photocatalyst becomes negative and repel Cr<sub>2</sub>O<sub>7</sub><sup>2-</sup> ions as reported by Padhi and Parida (2014). Table 2.4 summarises some of the reports on the removal of Cr(VI) by iron oxides. From the table,  $\alpha$ -Fe<sub>2</sub>O<sub>3</sub> is considered the best photocatalyst when it formed composite with other compound or loaded with clay.

Table 2.3: Comparison of photocatalytic reduction performance of different photocatalyst on Cr(VI)

Photocatalyst	Cr(VI) concentration	pH	Light source	Removal percent (%)	Removal time (minute)	Reference
Hydroxylated $\alpha$ -Fe <sub>2</sub> O <sub>3</sub>	20 mg/L	-	300W Xe arc lamp	24.8-70.2	60	(Wang et al., 2016)
Fe <sub>2</sub> O <sub>3</sub> -MoS <sub>2</sub> nanocomposite	5 mg/L	-	500 W high-pressure halogen lamp	~100	120	(Zhang et al., 2016)
$\alpha$ -Fe <sub>2</sub> O <sub>3</sub> /aMEGO $\alpha$ -Fe <sub>2</sub> O <sub>3</sub>	10 mg/L	2	300W Xenon lamp	95.28 25.26	160	(Du et al., 2015)
$\alpha$ -FeOOH/RGO composite	10 mg/L	2-12	Visible light	11-94	180	(Padhi and Parida, 2014)
Fe <sub>2</sub> O <sub>3</sub> loaded clay	50 – 200 mg/L	2	Visible light	60-100	180	(Mekatel et al., 2012)
Fe <sub>3</sub> O <sub>4</sub> -stabilized Fe <sup>0</sup> nanoparticles	20 mg/L	5.5	-	17-47.8	120	(Wu et al., 2009)
Iron doped titania	$2.2 \pm (0.1) \times 10^{-4}$ mol/dm <sup>3</sup>	6.5	250W xenon lamp	15-45	30	(Navío et al., 1998)

## 2.4 Nanostructure Oxide Material

International Organization for Standardization has defined nanomaterial as material with structure either internal or surface is in nanoscale (ISO, 2011). The nanoscale mentioned is referred as size ranging around 1 to 100nm (Sutariya and Pathak, 2014). Nanomaterials can be categorised as: zero-dimensional (0-D), one-dimensional (1-D), two-dimensional (2-D) and three-dimensional (3-D) according to the number of

dimensions that are confined to nanoscale range. Material in nanoscale is expected to have greater relative surface area and greater surface area to volume ratio than their bulk form which results in highly reactive surface of the material with the surrounding (Sutariya and Pathak, 2014).

One-dimensional nanomaterial is material have one dimension that is not in the nanoscale range. One-dimensional structures include nanowires, nanorods, nanobelts and nanotubes whose lateral dimensions are in nanoscale range (Xia et al., 2003). Two-dimensional nanostructured materials are materials that have one dimension in nanoscale range. Two-dimensional structures include nanofilm, nanoplate and nanosheet. Three-dimensional nanomaterial is material composed of consolidated equiaxed crystallites or bulk structure comprised of nanoscale microstructure such as the building blocks are of few nanometers throughout the bulk structure.

Nanostructured metal-oxides have received great interest owing to their potential applications as catalysis, field effect transistor, gas sensor and energy storage (Choopun et al., 2010). 1-D nanostructured materials such as oxides with the form of nanowire and nanobelt have been utilised to produce electronic or optical device for the application in production of renewable energy (Yang et al., 2010). 2-D nanostructure oxides are also being explored for wide range of applications, include battery and supercapacitor applications. Wu et al. have reported the synthesis of iron oxide nanosheet as electrode for lithium-ion batteries (Wu et al., 2011). While 3-D nanostructure with hierarchically self-assembled structures has been studied by Zhong et al. for water treatment application (Zhong et al., 2006).